Chemosphere 291 (2022) 133074

Contents lists available at ScienceDirect

Chemosphere

journal homepage: www.elsevier.com/locate/chemosphere

Atomic-level insight into effect of substrate concentration and relative humidity on photocatalytic degradation mechanism of gaseous styrene

Jiangyao Chen [a,b], Liyun Zhang [a], Weikun Zhu [a], Guiying Li [a,b], Taicheng An [a,b,*]

[a] Guangdong Key Laboratory of Environmental Catalysis and Health Risk Control, Guangdong Technology Research Center for Photocatalytic Technology Integration and Equipment Engineering, Institute of Environmental Health and Pollution Control, Guangdong University of Technology, Guangzhou, 510006, China
[b] Guangzhou Key Laboratory of Environmental Catalysis and Pollution Control, Guangdong-Hong Kong-Macao Joint Laboratory for Contaminants Exposure and Health, School of Environmental Science and Engineering, Guangdong University of Technology, Guangzhou, 510006, China

HIGHLIGHTS

- Favored formation of product by higher styrene concentration and lower RH.
- Gaseous products from catalyst desorption further exchange oxygen atom with $H_2{}^{18}O$.
- RH highly enhances ^{18}O distribution in product than substrate concentration.
- Reaction of styrene with $O_2^{\cdot-}$ and $^1O_2$ (or ·OH) is dominated at low (or high) RH.
- Hydration is an important gaseous conversion pathway of product.

GRAPHICAL ABSTRACT

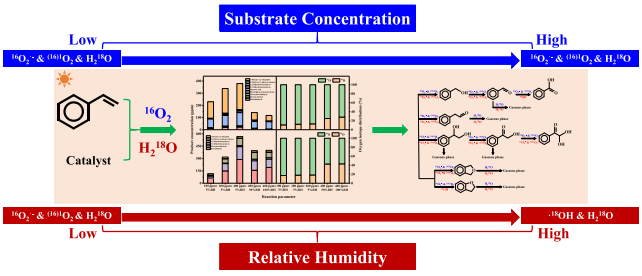

ARTICLE INFO

Handling editor: Junfeng Niu

Keywords:
Aromatic hydrocarbons
Advanced oxidation process
Reaction condition
Reactive oxygen species
Oxygen atom tracing

ABSTRACT

Substrate concentration and relative humidity (RH) impact the photocatalytic efficiency of industrial aromatic hydrocarbons, but how they influence intermediate formation and degradation pathway remains unclear. With the help of oxygen isotope tracing method, the effects of these two environmental parameters on degradation mechanism of styrene were revealed at atomic level. Increasing styrene concentration favored product formation, which was however inhibited by RH elevation. Gaseous products were not directly formed in gaseous phase, but originated from desorption of interfacial intermediates. The volatile aldehydes and furans further exchanged their ^{16}O with ^{18}O in $H_2{}^{18}O$. Increase of RH showed higher enhancement on ^{18}O distribution in all products and pathways than that of substrate concentration. Low RH preferred high generation of $^{16}O_2{}^{\bullet-}$ and $^{(16)1}O_2$, dominating reaction to form 1-phenyl-1,2-ethandiol, 2-hydroxy-1-phenyl-ethanon and phenylglyoxal monohydrate in sequence. Successive production of benzyl alcohol, benzaldehyde and benzoic acid through the reaction of styrene with promoted $^{\bullet18}OH$ by increasing RH became predominant. Hydration was firstly observed and confirmed as an important gaseous transformation step of aldehyde and furan products. Our findings provide a deep insight into photocatalytic degradation mechanism of aromatic hydrocarbons regulated by environmental parameters to further improve their industrial purification efficiency, and are helpful predicting environmental geochemistry fate of organics and preventing their negative impact on natural environment.

* Corresponding author. Guangdong Key Laboratory of Environmental Catalysis and Health Risk Control, Guangdong Technology Research Center for Photocatalytic Technology Integration and Equipment Engineering, Institute of Environmental Health and Pollution Control, Guangdong University of Technology, Guangzhou, 510006, China.
E-mail address: antc99@gdut.edu.cn (T. An).

https://doi.org/10.1016/j.chemosphere.2021.133074
Received 5 October 2021; Received in revised form 22 November 2021; Accepted 23 November 2021
Available online 25 November 2021

1. Introduction

Industrial chemical reaction processes such as polymer processing, plastic synthesis and petroleum refining discharge a large number of aromatic hydrocarbons (AHs). These AHs then diffuse into outdoor atmosphere and indoor environment, posing direct threat to ecosystem and human health (Babaee et al., 2010; Kim et al., 2011). AHs have received extensive attention from researchers and public, since their complex transformation process after emission, further impacting air quality (Guo et al., 2004; Li et al., 2014) and initiating cancer risk on human body (Bolden et al., 2015; Gonzalez-Martin et al., 2021; McKenzie et al., 2012; Minella and Minero, 2021). During the transformation process of AHs, many products will be generated, increasing type and toxicity of pollutants (Mo et al., 2009; Sun et al., 2010). Therefore, AHs shall be strictly controlled and efficiently treated to ensure their emission below toxic levels. As an advanced oxidation process with no secondary pollution and convenient operation, heterogeneous photocatalytic oxidation has been widely applied in decomposition of AHs (Al-Mamun et al., 2019; Oturan and Aaron, 2014; Pelaez et al., 2012). Thus, revealing photocatalytic degradation process of AHs is helpful for better regulation of treatment technique, improvement of oxidation efficiency and even elimination of health risk.

In general, the catalyst absorbs photon to generate h^+ and e^- after light irradiation, and then produces reactive oxygen species (ROS), such as $^{\bullet}OH$ and $O_2^{\bullet-}$, through redox reaction with H_2O and O_2. $O_2^{\bullet-}$ is further converted to $^1O_2$ or $^{\bullet}OH$ via the reaction with h^+, e^- or H_2O. Finally, AHs are degraded and mineralized by these ROS (Al-Mamun et al., 2019; Fotiou et al., 2016; Guo et al., 2015; Pelaez et al., 2012; Vali et al., 2020). The formation of ROS and its oxidation process toward AHs is certainly influenced by experimental parameters, such as substrate concentration and relative humidity (RH). Cheng et al. reported that conversion efficiency of ethylbenzene decreased as its initial concentration increased, while gradually enhanced when RH increased (Cheng et al., 2013b). Other authors observed similar phenomena during photocatalytic degradation of benzene (Doucet et al., 2007), toluene (Jafari et al., 2020), or o-xylene (Fu et al., 2019). Although lack of solid evidence, they deduced that insufficient ROS for high concentrated AHs and increased ROS at high RH were observed responsible for different variation of conversion efficiency, respectively.

In addition, the altered conversion efficiency of AHs by regulating substrate concentration or RH results in further influence of intermediate production. Quici et al. reported that dry air condition led to lower production of formaldehyde than humid one during toluene oxidation (Quici et al., 2010). The elevated RH increased accumulation of benzyl alcohol but decreased that of benzaldehyde during the oxidation of toluene (Guo et al., 2008). When increasing toluene concentration, oligomeric and polymeric intermediates were newly formed together with ring-opening ones (Einaga et al., 2013). However, they did not prove whether the alternation of intermediate formation is contributed from variation of ROS or experimental parameter. Actually, there exists somehow relationship among experimental parameter, ROS and degradation mechanism. Recently, by adjusting catalyst composition, we regulated the abundance of $^{\bullet}OH$ and $O_2^{\bullet-}$ to preliminarily achieve controlled production of intermediates (Chen et al., 2021; Wei et al., 2019). But, how the experimental parameter influences ROS formation and then degradation mechanism is still uncertain. To answer this question, tracing the migration route of oxygen atom from reaction species (e.g., H_2O, O_2) to ROS and then product was necessary (Bui et al., 2010, Li and Jenks, 2000; Oh et al., 2003; Pang et al., 2014; Xin et al., 2020; Zhang et al., 2009).

Thus, in this work, oxygen isotope tracing method was applied to investigate the effects of substrate concentration and RH on photocatalytic degradation mechanism of gaseous styrene. Styrene was selected as a representative AH, due to its wide utilization in synthesis and manufacture of polystyrene and other copolymers, leading to its massive emission in a variety of industrial effluents. The photocatalytic oxidation mechanism of styrene was revealed with elevated substrate concentration and RH when coexistence of $H_2{}^{18}O$ and $^{16}O_2$ at atomic level. The qualitative and quantitative analysis of gaseous and interfacial intermediates as well as their oxygen isotope distribution under different substrate concentration and RH was conducted by a gas chromatography-mass spectrometer (GC-MS). The formation process of three ROS ($^{\bullet}OH$, $O_2^{\bullet-}$, $^1O_2$) as well as evolution of their composition and intensity with elevated RH were studied. Photocatalytic degradation pathways of styrene were further explored in combination with the results of ROS and intermediates. Finally, the relationship of substrate concentration (or RH), ROS ($^{\bullet}OH$, $O_2^{\bullet-}$, $^1O_2$) with the degradation mechanism of styrene was established.

2. Experimental section

2.1. Photocatalytic degradation experiment

The designed amount of styrene and $H_2{}^{18}O$ was successively injected into a self-made Pyrex glass reactor (vol. 5 L) (Chen et al., 2019) filled with $^{16}O_2$ to achieve styrene concentration of 100, 200 and 400 ppmv, and RH of 5%, 50% and 100%. At the bottom of reactor, 150 mg of pretreated TiO_2 was uniformly dispersed on a clean Petri dish. After 30 min's dark equilibrium, a UV lamp (30 W, Guangdong Cnlight Co., Ltd.) with a maximum emission wavelength of 254 nm was turned on to vertically irradiate on the TiO_2 (P25, Degussa Company). Light intensity was measured as 0.38 mW cm^{-2}. After photocatalytic degradation for 60 min, TiO_2 was taken out for further analysis. The RH in the reactor was measured by a humidity/temperature measuring instrument (Testo 645, Germany) and showed small variations before and after reaction (Table S1). The concentration of CO_2 was analyzed by a gas chromatograph (GC-9800) equipped with methane converter.

2.2. Qualitative and quantitative analysis of intermediate

At 60 min, the gaseous products were analyzed by GC-MS (Agilent 7890B–5977B) with the help of solid-phase microextraction (SPME, 65 μm PDMS/DVB, Supelco). SPME fiber was pretreated for 6 min under temperature of 250 °C to remove residual organics and then sampled in the reactor for 10 min. The sampled fiber was taken out and quickly inserted into the injection port of GC-MS for analysis. The interfacial products were extracted via method reported recently (Chen et al., 2020a), and the collected solution was analyzed by GC-MS.

Qualitative analysis of gaseous and interfacial products was performed by comparing their ion fragment peaks with the National Institute of Standards and Technology (NIST) database and commercial compounds. Further quantification analysis of these products was conducted via calibration curve method. In brief, commercial compounds including benzaldehyde, benzyl alcohol, phenylacetaldehyde, benzoic acid, 2-hydroxy-1-phenyl-ethanon, 1-phenyl-1,2-ethandiol, 2,3-dihydrobenzofuran and 1,3-dihydrobenzofuran were used to quantitatively analyze their corresponding product compounds. 2-Hydroxy-1-phenyl-ethanon was applied to quantify phenylglyoxal monohydrate. The known amount of commercial compound was dissolved in ethyl acetate and directly analyzed by GC-MS. Detail preparation procedures and concentrations of standard compounds are given in Supporting Information.

2.3. Oxygen isotope distribution analysis of intermediate

The isotope percentages of ^{18}O and ^{16}O in intermediates were calculated based on ion fragment peak of products. The results were corrected with the oxygen isotope abundance of solvent H_2O and the natural isotope abundance of the product via Eqs. (1) and (2) (Li et al., 2012b). In these equations, C_p, C_n, C_w were ^{18}O percentages of measured isotope abundance of the product, natural isotope abundance of the product and ^{18}O percentage of solvent H_2O. All C_n is found less than

0.85% (Table S2), indicating very low natural isotope abundance of commercial compounds.

$$H_2O\% = 100 \times (C_p\text{-}C_n)/(C_w\text{-}C_n) \quad (1)$$

$$O_2\% = 100 \times (C_w\text{-}C_p)/(C_w\text{-}C_n) \quad (2)$$

2.4. ROS analysis under varied RH

Electron parameter resonance (EPR, Bruker EMXPlus-10/12) was applied to characterize ROS in simulated reaction systems. Typically, 150 mg of TiO_2 was added into 100 mM 5,5-dimethyl-1-pyrroline *N*-oxide (DMPO) acetonitrile solution for $^{\bullet}OH$, DMPO-methanol solution for $O_2^{\bullet-}$ or 2,2,6,6-tetramethyl-4-piperidone hydrochloride (TEMP) for $^1O_2$. Then, a certain amount of H_2O was added to simulate different RH. After 10 min's irradiation, 100 μL solution was taken out, filtered, capillary sampled and measured. Notably, a maximum of 90% RH was achieved for $O_2^{\bullet-}$ detection to prevent interference of $^{\bullet}OH$.

3. Results and discussion

3.1. Intermediate formation and its oxygen isotope distribution under the conditions of 400 ppmv styrene and 5% RH

First, photocatalytic degradation of 400 ppmv styrene was conducted with the presence of $H_2{}^{18}O$ (5% RH) and $^{16}O_2$. After 60 min, the white TiO_2 turns to yellow, implying generation of intermediates (d'Hennezel et al., 1998, Mendez-Roman and Cardona-Martınez, 1998). Analysis of extraction solution from the yellow TiO_2 by GC-MS reveals nine clear peaks (Fig. S1a), confirming formation of nine interfacial products. Further comparing mass fragments of peaks with the NIST library and commercial compound consistently confirms that these products are benzaldehyde, benzyl alcohol, phenylacetaldehyde, phenylglyoxal monohydrate, benzoic acid, 1,3-dihydrobenzofuran, 2, 3-dihydrobenzofuran, 2-hydroxy-1-phenyl-ethanon and 1-phenyl-1, 2-ethandiol (Figs. S2, S3 and Table S3). The number of intermediates is same no matter using $H_2{}^{18}O$ or $H_2{}^{16}O$ (Fig. S1c). The previous degradation of styrene produced partially same interfacial intermediates (Chen et al., 2019), supporting the current results.

In gaseous phase, a total of seven compounds are identified, including a mother compound (styrene) and six products (benzaldehyde, phenylacetaldehyde, 1,3-dihydrobenzofuran, 2,3-dihydrobenzofuran, 2-hydroxy-1-phenyl-ethanon and 1-phenyl-1,2-ethandiol) (Figs. S4a, S5 and Table S4). Interestingly, these six gaseous products are same as interfacial ones, implying that they are probably from catalyst desorption. Since UV lamp applied in this work is unable to decompose gaseous H_2O or O_2 to generate ROS (Chen et al., 2019), these oxygen containing products cannot directly form in gaseous phase. Conversely, they shall be firstly produced on the catalyst and then desorbed to the gaseous phase.

Further quantitative analysis of interfacial and gaseous products is carried out. Correlation coefficients (R^2) of all calibration curves for the standard compounds are >0.97, indicating reliability of quantitative method (Tables S5, S6; Figs. S6 and S7). The concentration and percentage of the interfacial products are shown in Fig. 1a, S8a and Table S7. Degradation of styrene produces 379.4 mg L^{-1} of intermediates on the catalyst. While 1-phenyl-1,2-ethandiol shows the highest concentration (214.0 mg L^{-1}) and percentage (56.41%). Followed by benzoic acid (107.6 mg L^{-1}), with the percentage of 28.36%. 1-Phenyl-1,2-ethandiol and benzoic acid account for higher than 84% percentage of total intermediates, suggesting main production of them on catalyst from styrene degradation. Previous studies also validated the production of these two products on catalyst from photocatalytic degradation of styrene, but without giving comparable quantification results (Chen et al., 2019; Shah et al., 2020).

Meanwhile, the gaseous intermediates are calculated as 566.3 mg L^{-1}, about 1.5 times of that on catalyst, indicating a large amount of intermediates discharging from catalyst to gas. The top three gaseous products in concentration are benzaldehyde (288.7 mg L^{-1}), phenylacetaldehyde (155.5 mg L^{-1}) and 2,3-dihydrobenzofuran (87.6 mg L^{-1}) (Fig. 1b). They contribute for higher than 93% of percentage in total intermediates, suggesting main desorption of them from catalyst surface (Fig. S9a). The different top concentrated products in gas and on catalyst is due to higher vapor pressure of benzaldehyde, phenylacetaldehyde and 2,3-dihydrobenzofuran than 1-phenyl-1,2-ethandiol and benzoic acid.

Furthermore, the oxygen isotope distribution of interfacial and gaseous products is discussed. Since there is no molecular ion peak for phenylglyoxal monohydrate, its fragment peaks are accordingly analyzed (Fig. S3). Based on the oxygen isotope distribution results (Fig. 1c and d), the average percentages of ^{16}O and ^{18}O in products from catalyst are 87% and 13%, while that from gaseous phase are 82% and 18%. The very close oxygen isotope distribution again confirms that the products in gas and on catalyst are homologous. Since $H_2{}^{18}O$ and $^{16}O_2$ show different oxygen isotope distribution, the much higher average percentage of ^{16}O than ^{18}O in products indicates that higher contribution of O_2 to the formation of these intermediates. However, the role of H_2O cannot be ignored, since ^{18}O proportions in interfacial benzyl alcohol, benzoic acid and 2,3-dihydrobenzofuran, and gaseous phenylacetaldehyde and 1,3-dihydrobenzofuran are over 22% and 25% (Figs. S8a and S9a), respectively. Previous works also reported the significance of H_2O in formation of some products (Cheng et al., 2014; Kunene et al., 2020), partially supporting present results.

3.2. Effect of substrate concentration on intermediate formation and its oxygen isotope distribution

Increasing substrate concentration to a certain extent always leads to decrease of degradation efficiency (Lyu et al., 2020; Mamaghani et al., 2018), which may influence formation of intermediate. As Fig. S1a shows, same nine interfacial intermediates are obtained at styrene concentrations of 400 and 200 ppmv, while 1,3-dihydrobenzofuran (No. 6) disappears when the concentration further decreases to 100 ppmv. Both 1,3-dihydrobenzofuran (No. 3) and 2-hydroxy-1-phenyl-ethanon (No. 5) are not detected in gaseous phase when the concentration decreases from 200 to 100 ppmv (Fig. S4a). These intermediates may show very low concentrations that are below the detection line of GC-MS, suggesting that low substrate concentration is not beneficial for forming partial intermediates.

The continuously decreased concentrations of intermediates from 379.4, 338.5 to 230.0 mg L^{-1} on catalyst and from 566.3, 317.8 to 115.6 mg L^{-1} in gas are observed at 400, 200 and 100 ppmv concentration of styrene, respectively (Fig. 1a and b). This indicates positively correlated variation between substrate concentration and intermediate production. The concentration of total intermediates increases by 89.9% from 100 to 200 ppmv and by 44.1% from 200 to 400 ppmv, revealing slower product formation at higher substrate concentration. This may be due to that the accumulated intermediates cover active site of catalyst and block absorption of photon to produce ROS (Ahmadpour et al., 2020; Ahmed et al., 2010; Mohanta and Ahmaruzzaman, 2020), and eventually reduce degradation efficiency of styrene.

Similar to that at 400 ppmv, the concentrations of 1-phenyl-1,2-ethandiol (202.0 and 135.2 mg L^{-1}) and benzoic acid (88.0 and 72.4 mg L^{-1}) still rank first and second places at 200 and 100 ppmv, accounting for 59.67%, 58.80% and 25.99%, 31.49% of total interfacial intermediates (Fig. 1a, S8b, S8c and Table S7). Besides these two products, the percentages of rest intermediates obtained within 100–400 ppmv are close, suggesting weak effect of substrate concentration to the proportion of most interfacial intermediates. Anyway, 1-phenyl-1,2-ethandiol and benzoic acid are two main intermediates on catalyst from degradation of styrene, no matter the variation of substrate

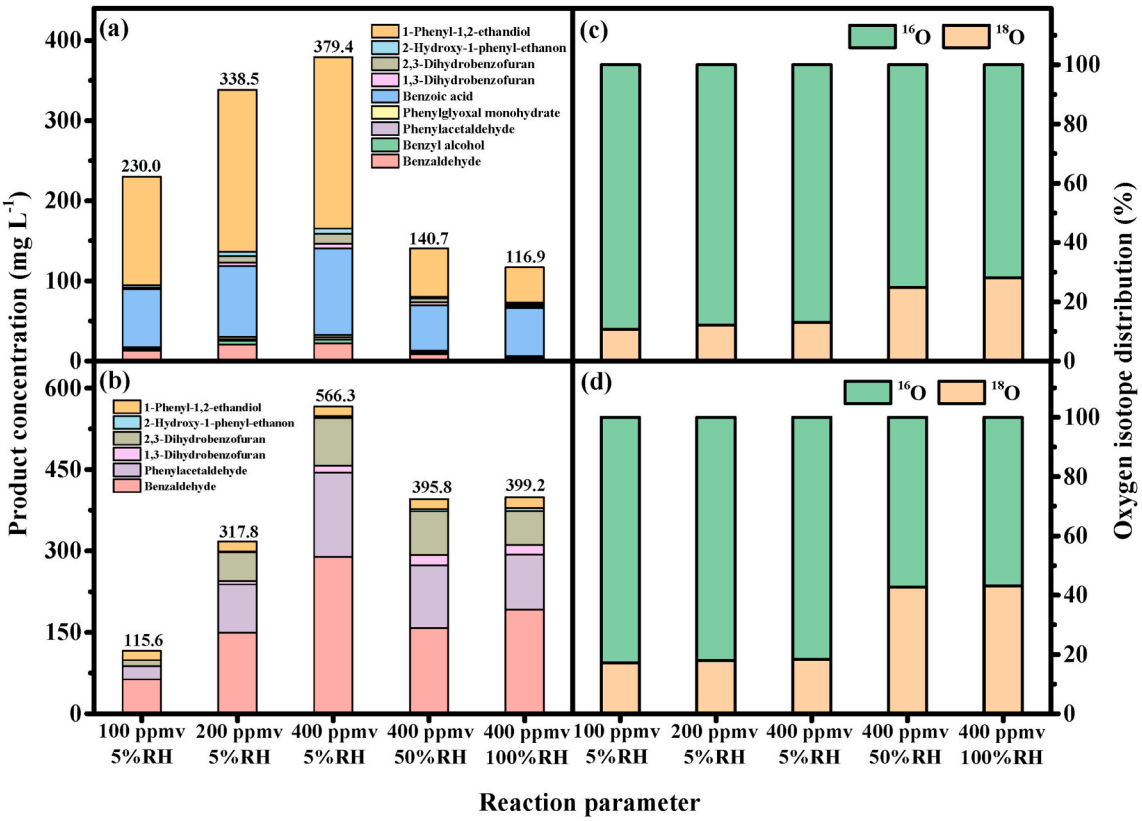

Fig. 1. Concentration and oxygen isotope distribution of interfacial (a, c) and gaseous (b, d) products after degradation of styrene at different substrate concentration and RH.

concentration. Chen et al. reported highly selective photocatalytic transformation of styrene to aromatic alcohol (Chen et al., 2020d), partially supporting present results.

Consistent with that at 400 ppmv, gaseous benzaldehyde (149.4 mg L^{-1}), phenylacetaldehyde (88.9 mg L^{-1}) and 2,3-dihydrobenzofuran (52.8 mg L^{-1}) also show the top three highest concentrations at 200 ppmv, with percentages of 47.02%, 27.98% and 16.62%, respectively (Fig. 1b, S9b and Table S8). Benzaldehyde and phenylacetaldehyde still possess the top two highest concentrations (63.4 and 24.4 mg L^{-1}) and percentages (54.84% and 21.11%) at 100 ppmv. However, the concentration and percentage of 2,3-dihydrobenzofuran sharply decrease to 10.7 mg L^{-1} and 9.26%, while 1-phenyl-1,2-ethandiol becomes the third highest concentration (17.1 mg L^{-1}) and percentage (14.79%) (Fig. 1b, S9c and Table S8). The more stable desorption of 1-phenyl-1,2-ethandiol from catalyst surface takes the responsibility. Anyway, benzaldehyde is the main gaseous intermediate from degradation of styrene, no matter the variation of substrate concentration.

Increasing substrate concentration may also lead to changed distribution of oxygen isotope in products. As shown in Fig. 1c and d, the average ^{18}O proportions of interfacial and gaseous products slightly increase from 10.7% to 13.0% and 17.2%–18.3% when styrene concentration is elevated from 100 to 400 ppmv. Increasing styrene concentration weakly promotes the ^{18}O distribution in products. Li et al. reported that higher initial concentration increased percentage of O-atom from $H_2{}^{18}O$ in hydroxylated intermediates from photocatalytic degradation of aqueous aromatic pollutants (Li et al., 2012a), agreeing with current result. Meanwhile, higher ^{18}O proportion of products in gas than on catalyst is observed, suggesting occurrence of exchange reaction between ^{18}O in $H_2{}^{18}O$ and ^{16}O in desorbed products. Shi et al. reported that hydration was responsible for incorporation of the O atom of H_2O into product during photocatalytic degradation of aldehydes (Shi et al., 2015), partially proving present result. However, deep mechanism for oxygen atom exchange reaction during styrene degradation is needed further investigation.

For interfacial products, their evolution of ^{18}O proportion along with elevated substrate concentration can be divided into three categories: slow increase, fast increase and decrease. The first category contains four products: benzoic acid, benzyl alcohol, phenylglyoxal monohydrate and 2-hydroxy-1-phenyl-ethanon. Their ^{18}O proportions separately increase from 21.0% to 24.6% (Fig. 2a), 17.2%–25.9% (Fig. S10a), 4.1%–8.6% (Fig. S10b), and 4.5%–8.2% (Fig. S10c) as styrene concentration increases from 100 to 400 ppmv. While 2,3-dihydrobenzofuran belongs to the second category and its ^{18}O percentage quadruples from 5.5% at 100 ppmv to 22.7% at 400 ppmv (Fig. 2b). However, 1,3-dihydrobenzofuran, its isomer in the third category, shows decreased trend of ^{18}O percentage (from 6.7% to 5.8%) (Fig. S10d). Elevating styrene concentration results in different distribution of ^{18}O in isomeric products. Similar to 1,3-dihydrobenzofuran, the decreased percentages of ^{18}O from 10.6% to 5.0% for 1-phenyl-1,2-ethandiol (Fig. 2c), 15.3%–13.9% for phenylacetaldehyde (Fig. S10e) and 7.1%–2.4% for benzaldehyde (Fig. S10f) are also obtained, respectively.

For gaseous products, the ^{18}O percentages in benzaldehyde (Fig. 2d) and 1,3-dihydrobenzofuran (Fig. S11b) increased from 24.1% to 30.2% and 23.0%–25.5%, while that in 2,3-dihydrobenzofuran (Fig. 2e), phenylacetaldehyde (Fig. S11a) and 2-hydroxy-1-phenyl-ethanon (Fig. S11c) decrease from 29.0% to 27.5%, 42.5%–38.9% and 3.2%–2.8%, respectively. Interestingly, gaseous 1-phenyl-1,2-ethandiol shows far lower ^{18}O percentage ($\leq$1.2%, Fig. 2f) than that on catalyst ($\geq$5.0%, Fig. 2c). This is probably due to that ^{16}O dominated 1-phenyl-1,2-ethandiol possesses higher vapor pressure than ^{18}O one, leading to easier vaporization of the former from catalyst surface. However, ^{16}O atom in desorbed 1-phenyl-1,2-ethandiol does not further exchange with ^{18}O in $H_2{}^{18}O$. Conversely, preferentially vaporized phenylacetaldehyde, benzaldehyde, 1,3-dihydrobenzofuran and 2,3-dihydrobenzofuran

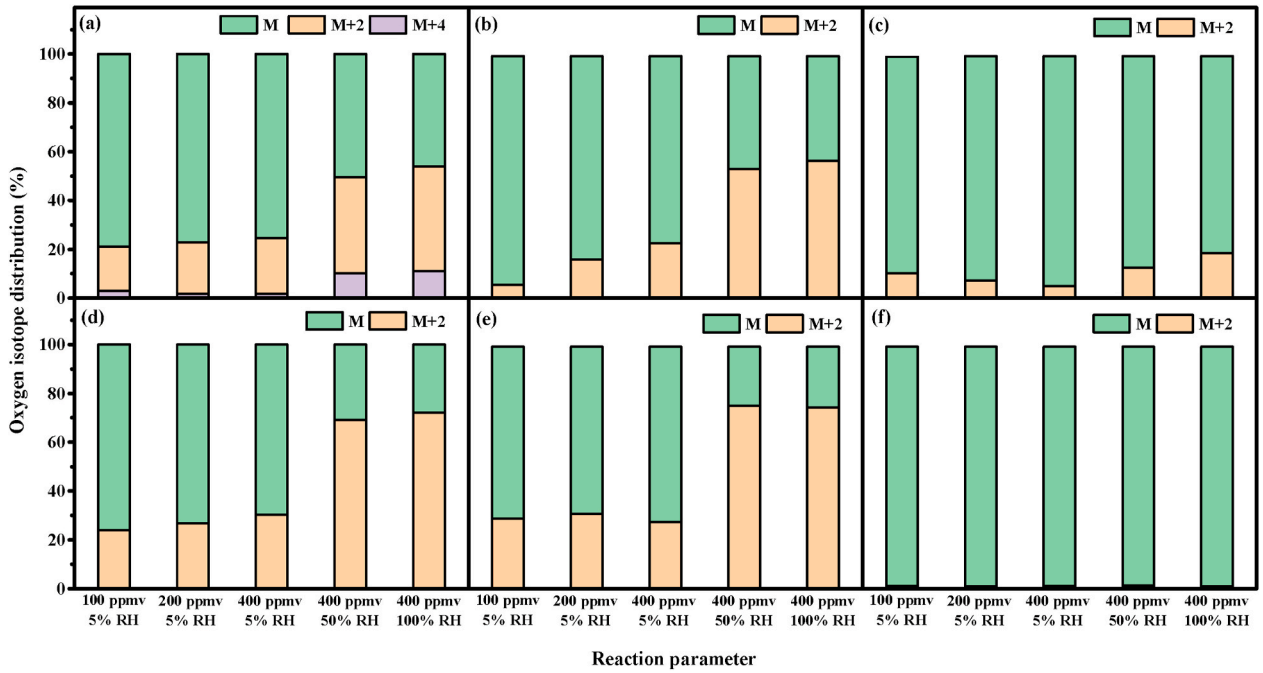

Fig. 2. Oxygen isotope distribution of interfacial (up) and gaseous (down) products obtained at different substrate concentration and RH ((a) benzoic acid, (b, e) 2,3-dihydrobenzofuran, (c, f) 1-phenyl-1,2-ethandiol and (d) benzaldehyde) (M, M+2 and M+4 indicate that zero, one and two ^{18}O atom are incorporated into the intermediates, respectively).

mainly labeled by ^{16}O favors hydration with $H_2{}^{18}O$, resulting in much higher ^{18}O percentages of them in gas than on catalyst.

3.3. Effect of RH on intermediate formation and its oxygen isotope distribution

Increasing RH from 5% to 100% does not vary composition of both interfacial and gaseous intermediates (Figs. S1b and S4b). However, the concentrations of interfacial and gaseous products sharply decrease from 379.4 to 140.7 mg L^{-1} and 566.3 to 395.8 mg L^{-1}, and then slowly change to 116.9 and 399.2 mg L^{-1} when RH increasing from 5% to 50% and 100% (Fig. 1a and b). The intermediate concentration shows similar variation trend on catalyst and in gas, again confirming origination of gaseous products from desorption of interfacial ones. Two reasons are responsible for the decreased formation of intermediates with elevated RH. First, higher RH makes more H_2O molecules to be oxidized by h^+ on catalyst to generate stronger oxidant $^{\bullet}OH$ and improves mineralization rate of styrene as well as its products (Guo et al., 2008; Shayegan et al., 2019). Second, the catalyst surface will be covered by plenty of H_2O molecules at high RH to form H_2O clusters, which occupy active sites to suppress formation of products (Cao et al., 2000; Shayegan et al., 2018). The sum concentration of interfacial and gaseous products obtained from 5% to 50% RH reduces 409.2 mg L^{-1}, which is 20.1 times of that from 50% to 100% RH (20.4 mg L^{-1}). This big disparity suggests that 50% RH ensures efficient mineralization of both styrene and its products. About 1020 ppm of CO_2 was produced at this RH, supporting the conclusion. Previous studies always reported an optimum mineralization preformation of gaseous organics at medium RH (Shayegan et al., 2020; Zhou et al., 2019), consistent with our results.

Similar to that at 5% RH, 1-phenyl-1,2-ethandiol (60.4 and 44.0 mg L^{-1}) and benzoic acid (56.8 and 60.0 mg L^{-1}) are still the top two concentrated intermediates on catalyst at 50% and 100% RH, accounting for 42.93% and 37.64%, and 40.38% and 51.33%, respectively (Fig. 1a, S8d, S8e and Table S7). The proportion of benzoic acid exceeds 1-phenyl-1,2-ethandiol at 100% RH, probably due to increased desorption of the latter to gaseous phase. Approximately 18.6 and 20.3 mg L^{-1} of 1-phenyl-1,2-ethandiol are detected in gaseous phase at 50% and 100% RH, confirming above hypothesis. In gaseous phase, benzaldehyde (157.6 and 191.9 mg L^{-1}), phenylacetaldehyde (115.9 and 101.2 mg L^{-1}) and 2,3-dihydrobenzofuran (80.8 and 62.7 mg L^{-1}) also show the top three highest concentrations at 50% and 100% RH, accounting for 39.82% and 48.07%, 29.28% and 25.35%, and 20.41% and 15.71% of total gaseous intermediates, respectively (Fig. 1b, S9d, S9e and Table S8). Benzaldehyde shows an enhanced concentration with elevation of RH from 50% to 100%, possibly due to its highest solubility in water.

For oxygen isotope distribution of intermediates, the average proportions of ^{18}O in interfacial and gaseous products increase from 13.0% to 18.3% at 5% RH to 24.9% and 42.7% at 50% RH, and then to 28.1% and 43.2% at 100% RH (Fig. 1c and d). Faster enhancement of ^{18}O percentage in products is observed from 5% to 50% RH than from 50% to 100% RH, suggesting that suitable RH efficiently increases ^{18}O distribution in all intermediates. The gaseous products display 40.8%–71.5% higher ^{18}O proportion than that on catalyst, mainly ascribing from hydration reaction of desorbed products with $H_2{}^{18}O$.

Consistent with results obtained at 5% RH, 2,3-dihydrobenzofuran (53.4% and 56.8%, Fig. 2b), benzoic acid (49.5% and 54.0%, Fig. 2a) and benzyl alcohol (44.3% and 39.6%, Fig. S10a) on catalyst, while 2,3-dihydrobenzofuran (75.6% and 75.0%, Fig. 2e), phenylacetaldehyde (73.7% and 72.1%, Fig. S11a) and benzaldehyde (69.2% and 72.2%, Fig. 2d) in gas separately show the top three highest percentages of ^{18}O at 50% and 100% RH. These results again confirm the important role of $H_2{}^{18}O$ in intermediate production. Notably, elevating RH from 5% to 100% increases ^{18}O percentage of 1,3-dihydrobenzofuran by 4.9% on catalyst and by 16.3% in gas (Figs. S10d and S11b), about seven and three times lower of 2,3-dihydrobenzofuran, suggesting selective participation of ^{18}O in formation of the latter.

Since increase of RH to a certain value will promote the formation of products such as benzoic acid during photocatalytic process of toluene and ethylbenzene (Cheng et al., 2014; Guo et al., 2008), the relationship between promoted H_2O and intermediate generation has never been explored. The differentiation of H_2O's contribution may be due to its different selectivity toward intermediate (Chen et al., 2020b), and this is closely determined by their reaction mechanism with H_2O, which still

remains unclear. Our findings experimentally reveal how H_2O content affects the formation and oxygen distribution of interfacial and gaseous intermediates during degradation of styrene, which may be helpful to unclose the reaction pathway and mechanism between H_2O and intermediate.

3.4. Degradation mechanism of styrene associated with substrate concentration and RH

Based on above intermediate (in gas and on catalyst) results and previous studies (Balachandramohan et al., 2020; Chen et al., 2019; Sheng et al., 2019), four degradation pathways of styrene are preliminarily proposed and shown in Fig. 3a. In pathway I, degradation of styrene produces benzyl alcohol, benzaldehyde and benzoic acid in turn, while only phenylacetaldehyde forms via pathway II. Styrene is sequentially converted to 1-phenyl-1,2-ethandiol, 2-hydroxy-1-phenyl-ethanon and phenylglyoxal monohydrate through pathway III. While two isomers of 1,3-dihydrobenzofuran and 2,3-dihydrobenzofuran are formed via pathway Ⅳ. At the meantime, benzaldehyde from pathway I, phenylacetaldehyde from pathway II, 1-phenyl-1,2-ethandiol and 2-hydroxy-1-phenyl-ethanon from pathway III, and 1,3-dihydrobenzofuran and 2,3-dihydrobenzofuran from pathway IV desorb from catalyst to gaseous phase. Then, the effects of substrate concentration and RH on degradation pathway of styrene are discussed based on concentration percentage and ^{18}O distribution of products.

At styrene concentration of 100 ppmv, the percentages of its products from four pathways are 43.46%, 7.44%, 45.43% and 3.67%, respectively (Fig. 3b). Pathways I and III are the two most important formation routes of products. With increasing the concentration to 200 and 400 ppmv, the product percentages accordingly change to 40.05% and 44.74% for pathway I, 13.88% and 16.74% for pathway II, 35.17% and 25.89% for pathway III, and 10.90% and 12.63% for pathway IV, respectively. The concentration percentage of products in pathway IV shows the fastest enhancement, due to formation of the new product, 1,3-dihydrobenzofuran. The pathway III still contributes much high product formation. Our recent work experimentally and theoretically confirmed initial transformation of styrene to 1-phenyl-1,2-ethandiol (Chen et al., 2019). Other researches verified that side chain oxidation pathway was primary in photocatalytic oxidation of o-xylene (Rao et al., 2020), while α-carbon oxidation pathway was dominant in degradation of ethylbenzene (Cheng et al., 2013a). Hence, degradation of styrene preferentially undergoes pathway III to initially form 1-phenyl-1,2-ethandiol and then other products under investigated substrate concentration and low RH (5%). However, the product proportion in pathway III is exceeded by that in pathway I with increasing styrene concentration, due to high concentrated benzaldehyde in gaseous phase.

Enlarged disparity of product proportion between pathway I (41.94% and 49.76%) and pathway III (16.12% and 14.01%) was obtained with increasing RH to 50% and 100%. The slower decreased formation of benzoic acid (main product in pathway I) than 1-phenyl-1,2-ethandiol (main product in pathway III) is responsible for this big disparity. At 5% RH, the production of 1-phenyl-1,2-ethandiol (232.0 mg L^{-1}) is about 2.2 times of benzoic acid (107.6 mg L^{-1}), while their disparity is only 1.1 times (64.3 vs 60.0 mg L^{-1}) at 100% RH (Fig. 1a and b). This is probably because that benzoic acid is the final product of pathway I and can be ceaselessly converted from benzaldehyde and benzyl alcohol. However, 1-phenyl-1,2-ethandiol is the first product of pathway III and must further transforms to 2-hydroxy-1-phenyl-ethanon and phenylglyoxal monohydrate. The higher increased concentration of benzaldehyde from pathway I than that of 1-phenyl-1,2-ethandiol and 2-

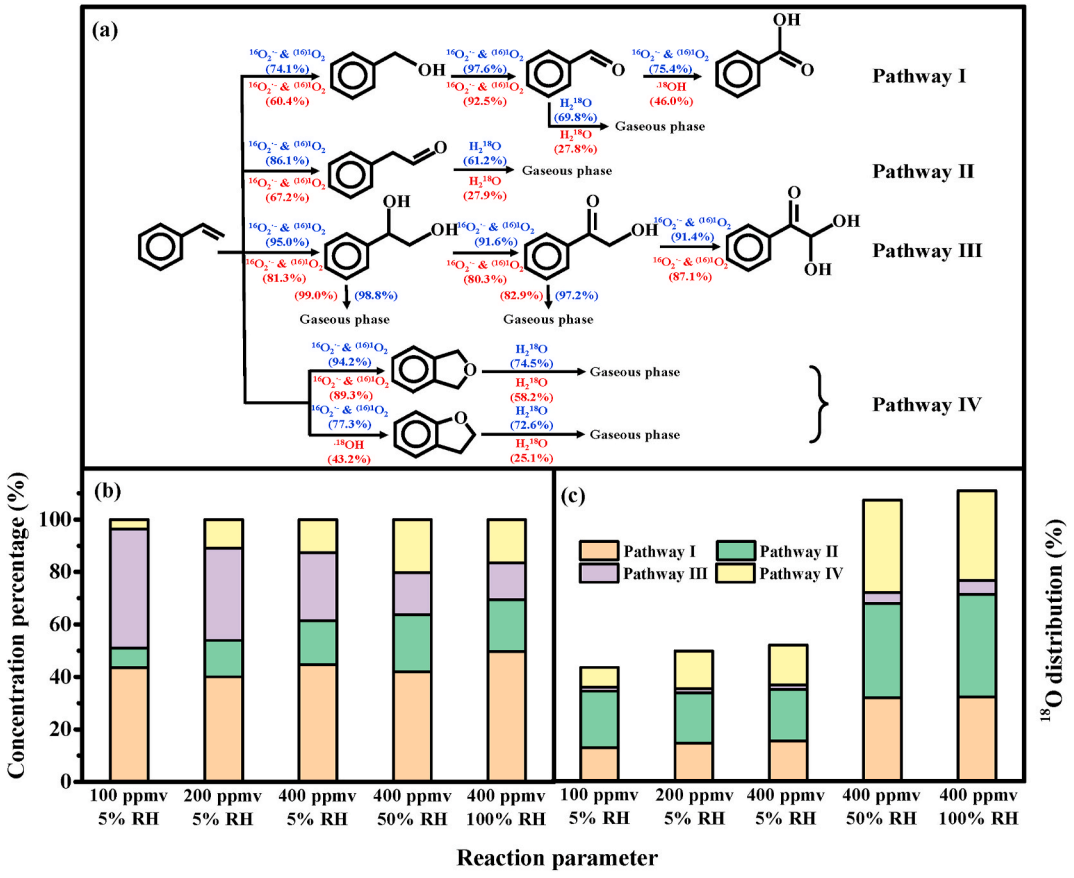

Fig. 3. (a) Dominated ROS involved degradation mechanism of 400 ppmv styrene under 5% (blue) and 100% RH (red) (number in bracket represents the ^{16}O percentage in product), and percentage of concentration (b) and ^{18}O (c) in products from four pathways at different substrate concentration and RH. (For interpretation of the references to colour in this figure legend, the reader is referred to the Web version of this article.)

hydroxy-1-phenyl-ethanon from pathway III in gas is another reason. In addition, the pathway II (21.78% and 19.71%) and IV (12.63% and 16.5%) show minor but stable percentages of products at both 50% and 100% RH, indicating weak effect of enhanced RH on intermediate production via these two pathways.

The average ^{18}O isotope distribution in products from four pathways under different substrate concentration and RH are also compared (Fig. 3c). When styrene concentration increases from 100 to 400 ppmv, the ^{18}O percentages in products of pathway I (from 17.3% to 20.7%), II (from 28.9% to 26.4%) and III (from 2.2% to 2.3%) show subtle variation, while that of pathway Ⅳ doubles from 10.0% to 20.4%. Combining with results in Fig. 3b, increased concentration of styrene promotes both concentration and ^{18}O distribution of products in pathway Ⅳ, due to new formation of 1,3-dihydrobenzofuran.

When RH increases from 5% to 50%, the ^{18}O percentages of products in all pathways increase (from 20.7% to 42.9% for pathway I, 26.4%–48.3% for pathway II, 2.3%–5.6% for pathway III, and 20.4%–47.3% for pathway IV). Further elevation of RH to 100% continuously increased ^{18}O proportions of products to 43.3%, 52.5% and 7.0% for pathway I, II and III, while slightly decreased that to 46.1% for pathway IV. Much higher promotion of ^{18}O distribution in products for all pathways is observed via enhanced RH than substrate concentration. The ^{18}O percentages in products generated through pathway I, II and IV are close and about six times higher than that through pathway III, suggesting that $H_2{}^{18}O$ does not prefer to participate into the product formation via the latter pathway. This result also gives solid evidence for lower percentage of products generated from pathway III than pathway I at higher RH. The relatively strong affinity of products from pathway I with H_2O should be responsible for above results (d'Hennezel et al., 1998; Sleiman et al., 2009).

The above results confirm more conspicuous significance of RH than substrate concentration during degradation of styrene. Hence, the effect of RH on degradation mechanism of styrene is further investigated. Since H_2O and O_2 in photocatalytic system are mainly converted to ROS (e.g., $^{\bullet}OH$, $O_2^{\bullet-}$ and $^1O_2$) and then degrade styrene to intermediates, the evolution of these ROS at different RH is firstly discussed. As shown in Fig. 4a, no signal of DMPO-OH is observed at 5% RH, indicating too low concentration of $^{\bullet}OH$ to be detected by EPR. The superimposed signals of alkoxy group and DMPO-O_2^- are observed under this experimental condition, due to the oxidation of impurity in DMPO and reduction of O_2 by electron (Long et al., 2012). Meanwhile, signals of DMPO-O_2^- and alkyl group are both detected at 5% RH in methanol system (Fig. 4b), confirming existence of $O_2^{\bullet-}$. The formation of alkyl group may come from oxidation of methanol (Michail and Siraki, 2012). The presence of $^1O_2$ is also proved from three distinct 1:1:1 characteristic peaks (Fig. 4c). Clearly, $^1O_2$ and $O_2^{\bullet-}$ are predominant at 5% RH.

As expected, four clear peaks of DMPO-OH with intensity ratio of 1:2:2:1 are observed at 50% RH (Fig. 4a), confirming enhanced formation of $^{\bullet}OH$ with elevated RH. The DMPO-OH signals show identical intensity at RH of 50% and 100%, indicating that further increase of RH does not promote the generation of $^{\bullet}OH$. The superimposed signals of alkyl group and DMPO-O_2^- are also observed at RH of 50% and 100% (Fig. 4b). Meanwhile, close intensities of DMPO-O_2^- signals are obtained at these RH, which are much lower than that at 5% RH. The generation of $O_2^{\bullet-}$ is significantly inhibited by increased RH. Also, decreased signals of TEMP-$^1O_2$ are observed when RH increases from 5% to 50% (Fig. 4c), revealing that higher RH suppresses the formation of $^1O_2$. This suppression is remarkably strengthened when RH achieves 100%, resulting in almost invisible signals of TEMP-$^1O_2$. Elevated RH significantly increases formation of $^{\bullet}OH$, but remarkably decreases that of both $O_2^{\bullet-}$ and $^1O_2$.

Based on previous researches (Al-Mamun et al., 2019; Chen et al., 2020c; Pelaez et al., 2012), the main generation routes of oxygen isotope labeling ROS from $H_2{}^{18}O$ and $^{16}O_2$ are proposed. Under 254 nm ultraviolet light irradiation, TiO_2 absorbs photon to form h^+ and e^- (Eq. (3)), which then separately oxidize $H_2{}^{18}O$ to $^{\bullet18}OH$ (Eq. (4)) and reduce $^{16}O_2$ to $^{16}O_2^{\bullet-}$ (Eq. (5)). The obtained $^{16}O_2^{\bullet-}$ is further oxidized by h^+ to $^{(16)}{}^1O_2$ (Eq. (6)). In the meantime, $^{16}O_2^{\bullet-}$ reacts with $H_2{}^{18}O$ to $^{\bullet18}OH$ (Eq. (7)) (Kim et al., 2002; Liang et al., 2020; Qiu et al., 2018). Fig. S12 shows a schematic drawing of ROS formation processes under low and high RH. Notably, $^{16}O_2^{\bullet-}$ mainly converts to $^{(16)}{}^1O_2$ at low RH (Eq. (6)), while increasing RH favors its transformation to $^{\bullet18}OH$ (Eq. (7)). The ^{16}O still dominates in $O_2^{\bullet-}$ and $^1O_2$ at both low and high RH (Eqs. (5) and (6)).

$$TiO_2 + h\nu \rightarrow h^+ + e^- \quad (3)$$

$$H_2{}^{18}O + h^+ \rightarrow {}^{\bullet18}OH + H^+ \quad (4)$$

$$^{16}O_2 + e^- \rightarrow {}^{16}O_2^{\bullet-} \quad (5)$$

$$^{16}O_2^{\bullet-} + h^+ \rightarrow {}^{(16)}{}^1O_2 \quad (6)$$

$$2\,{}^{16}O_2^{\bullet-} + 2H_2{}^{18}O \rightarrow 2\,{}^{\bullet18}OH + 2\,{}^{18}OH^- + {}^{16}O_2 \quad (7)$$

Fig. 3a displays ROS and $H_2{}^{18}O$ involved degradation mechanism of styrene. The blue or red marked $^{16}O_2^{\bullet-}$, $^{(16)}{}^1O_2$, $^{\bullet18}OH$ or $H_2{}^{18}O$ means their dominantly contribution to the followed product under 400 ppmv styrene with 5% or 100% RH. The ^{16}O isotope percentage in the formed product is also listed in the bracket. As shown in the figure, the ^{16}O percentages in products of four pathways range from 61.2% to 98.8% at 5% RH, indicating main participation of $^{16}O_2^{\bullet-}$ and $^{(16)}{}^1O_2$ into styrene degradation of this study. However, their participation is weakened as RH elevates. The average ^{18}O proportions in interfacial and gaseous products of pathway I, II and IV are 33.7% and 72.2%, 32.8% and 72.1%, and 23.1% and 58.3% at 100% RH, revealing significance contribution of $^{\bullet18}OH$ and $H_2{}^{18}O$ in the formation of these products. Comparatively, the products from pathway III show the lowest average proportion of ^{18}O (5.2% at 5% RH and 13.9% at 100% RH), suggesting the most difficult participation of $^{\bullet18}OH$ and $H_2{}^{18}O$ in their formation. At low RH, $^{16}O_2$ is more easily reduced by e^- to form $^{16}O_2^{\bullet-}$ via Eq. (5) and then oxidizes to $^{(16)}{}^1O_2$ by h^+ via Eq. (6). However, the latter process is supressed at high RH, leading to low formation of $^{(16)}{}^1O_2$ with

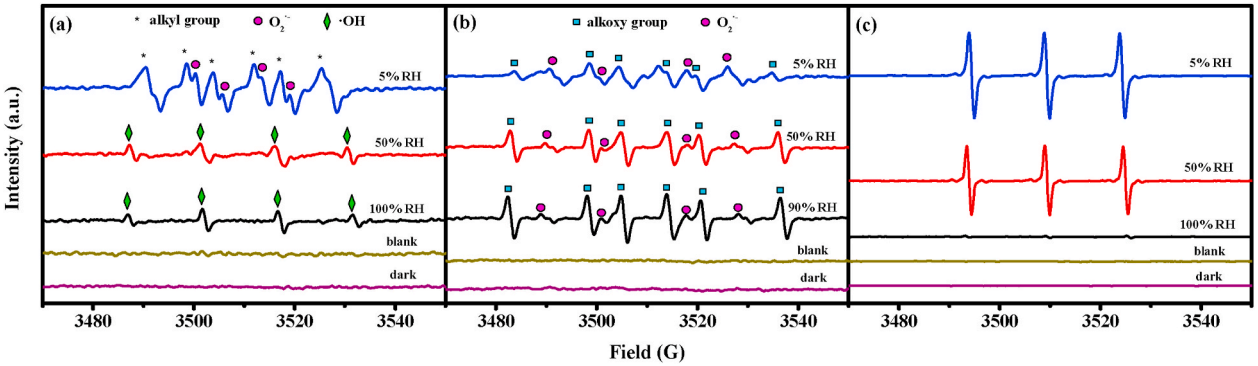

Fig. 4. Evolution of ·OH (a), $O_2^{\cdot-}$ (b) and $^1O_2$ (c) at different RH.

highly residual concentrated h^+ and $^{16}O_2^{\bullet-}$. Finally, these two reactive species react with $H_2{}^{18}O$ to produce high intensity of $^{\bullet 18}OH$ via Eqs. (4) and (7).

As for individual interfacial product, the high ^{16}O percentages in phenylacetaldehyde (from 86.1% to 67.2%) from pathway II, and 1-phenyl-1,2-ethandiol (from 95.0% to 81.3%) and 2-hydroxy-1-phenyl-ethanon (from 91.6% to 80.3%) from pathway III indicate that they are mainly from the reaction of styrene with $^{16}O_2^{\bullet-}$ and $^{(16)1}O_2$ via Eqs. (5) and (6). Previous research has proposed the formation of above three products via reaction of $^{\bullet}OH$ and styrene (Chen et al., 2019). However, the deduction of this conclusion is only based on ROS characterization results. Although our EPR results also confirm the enhanced formation of $^{\bullet}OH$ with elevated RH, the oxygen isotope distribution results reveal the dominant ^{16}O percentage. This means that styrene actually reacts with $^{16}O_2^{\bullet-}$ and $^{(16)1}O_2$ rather than $^{\bullet 18}OH$ to form above products. Since the amount of $^{16}O_2$ is much higher than $H_2{}^{18}O$ in the study, the total production of $^{16}O_2^{\bullet-}$ and $^{(16)1}O_2$ shall be far higher than that of $^{\bullet 18}OH$, leading to main contribution of the former to those products.

Same phenomenon is obtained on benzyl alcohol (from 74.1% to 60.4%) and benzaldehyde (from 97.6% to 92.5%) in pathway I. However, with elevating RH from 5% to 100%, the reaction of $^{\bullet 18}OH$ with benzaldehyde becomes dominant on catalyst, doubling the percentage of ^{18}O in benzoic acid from 24.6% to 54.0%. As known, OH-addition always happens on transformation of benzaldehyde to benzoic acid (Chen et al., 2020e; Shayegan et al., 2018). At higher RH, the formation of $^{\bullet 18}OH$ is enhanced via Eqs. (4) and (7), and then oxidizes benzaldehyde to benzoic acid with increased ^{18}O percentage. Interestingly, OH-addition on styrene form two isomers, 1,3-dihydrobenzofuran and 2,3-dihydrobenzofuran, which contain totally different distributions of ^{16}O (89.3% and 43.2%) at 100% RH. This result suggests that selective $^{\bullet 18}OH$ addition on styrene to form 2,3-dihydrobenzofuran rather than 1,3-dihydrobenzofuran.

After reaction with different ROS to form products on catalyst, part of them will desorb and diffuse into the gaseous phase to trigger hydration reaction with $H_2{}^{18}O$. At 5% RH, the percentages of ^{16}O in benzaldehyde from pathway I, phenylacetaldehyde from pathway II, 1,3-dihydrobenzofuran and 2,3-dihydrobenzofuran from pathway IV range from 61.2% to 74.5%, far lower than that on catalyst (from 77.3% to 97.6%), confirming exchange of ^{16}O in these products by ^{18}O in $H_2{}^{18}O$. This exchange is further boosted with RH increasing to 100% that the range of their ^{16}O percentages is only from 25.1% to 58.2%. However, 1-phenyl-1,2-ethandiol (98.9% in average) and 2-hydroxy-1-phenyl-ethanon (90.1% in average) from pathway III still show high ^{16}O percentages as that on catalyst, indicating difficult oxygen exchange between them and $H_2{}^{18}O$. This is the first time that observes and confirms hydration reaction of aldehyde and furan products in gaseous phase during photocatalytic degradation of styrene. These findings provide a deep and comprehensive photocatalytic degradation mechanism of styrene and are helpful to further improve its purification efficiency.

4. Conclusions

In present work, the effect of substrate concentration and RH to the photocatalytic degradation intermediate, pathway and mechanism of gaseous styrene was studied based on oxygen isotope tracing method. The production of intermediates was enhanced by the increasing styrene concentration, while elevating RH inhibited product formation. The RH showed higher enhancement on ^{18}O distribution in all products and pathways than substrate concentration. $^{16}O_2^{\bullet-}$, $^{(16)1}O_2$ and $^{\bullet 18}OH$ displayed different dominant contribution during degradation of styrene to its products. Hydration was solidly confirmed as an important gaseous transformation step of aldehyde and furan products, due to oxygen exchange of them with $H_2{}^{18}O$. These results provided a new understanding toward photocatalytic degradation mechanism of AHs by monitoring experimental conditions to alter their intermediates, and emphasized the necessity to predict environmental geochemistry fate of AHs to alleviate their negative impact on natural environment with different reactive oxygen species.

Credit author statement

Jiangyao Chen: Formal analysis, Methodology, Writing – original draft. **Liyun Zhang**: Formal analysis, Methodology. **Weikun Zhu**: Investigation. **Guiying Li**: Validation. **Taicheng An**: Conceptualization, Supervision.

Declaration of competing interest

The authors declare that they have no known competing financial interests or personal relationships that could have appeared to influence the work reported in this paper.

Acknowledgements

This work was financially supported by NSFC (21777032, 42177354), National Key R&D Program of China (2019YFC0214402), Key-Area Research and Development Program of Guangdong Province (2019B110206002), and Local Innovative and Research Teams Project of Guangdong Pearl River Talents Program (2017BT01Z032).

Appendix A. Supplementary data

Supplementary data to this article can be found online at https://doi.org/10.1016/j.chemosphere.2021.133074.

References

Ahmadpour, N., Sayadi, M.H., Sobhani, S., Hajiani, M., 2020. Photocatalytic degradation of model pharmaceutical pollutant by novel magnetic TiO_2@$ZnFe_2O_4$/Pd nanocomposite with enhanced photocatalytic activity and stability under solar light irradiation. J. Environ. Manag. 271, 110964.

Ahmed, S., Rasul, M.G., Martens, W.N., Brown, R., Hashib, M.A., 2010. Heterogeneous photocatalytic degradation of phenols in wastewater: a review on current status and developments. Desalination 261 (1–2), 3–18.

Al-Mamun, M.R., Kader, S., Islam, M.S., Khan, M.Z.H., 2019. Photocatalytic activity improvement and application of UV-TiO_2 photocatalysis in textile wastewater treatment: a review. J. Environ. Chem. Eng 7 (5), 103248.

Babaee, R., Bonakdarpour, B., Nasernejad, B., Fallah, N., 2010. Kinetics of styrene biodegradation in synthetic wastewaters using an industrial activated sludge. J. Hazard Mater. 184 (1–3), 111–117.

Balachandramohan, J., Sivasankar, T., Sivakumar, M., 2020. Facile sonochemical synthesis of Ag_2O-guar gum nanocomposite as a visible light photocatalyst for the organic transformation reactions. J. Hazard Mater. 385, 121621.

Bolden, A.L., Kwiatkowski, C.F., Colborn, T., 2015. New look at BTEX: are ambient levels a problem? Environ. Sci. Technol. 49 (9), 5261–5276.

Bui, T.D., Kimura, A., Ikeda, S., Matsumura, M., 2010. Determination of oxygen sources for oxidation of benzene on TiO_2 photocatalysts in aqueous solutions containing molecular oxygen. J. Am. Chem. Soc. 132 (24), 8453–8458.

Cao, L.X., Gao, Z., Suib, S.L., Obee, T.N., Hay, S.O., Freihaut, J.D., 2000. Photocatalytic oxidation of toluene on nanoscale TiO_2 catalysts: studies of deactivation and regeneration. J. Catal. 196 (2), 253–261.

Chen, J.Y., He, Z.G., Ji, Y.M., Li, G.Y., An, T.C., Choi, W.Y., 2019. (OH)-O-center dot radicals determined photocatalytic degradation mechanisms of gaseous styrene in TiO2 system under 254 nm versus 185 nm irradiation: Combined experimental and theoretical studies. Appl. Catal. B: Environ 257, 117912.

Chen, J.Y., Yi, J.J., Ji, Y.M., Zhao, B.C., Ji, Y.P., Li, G.Y., An, T.C., 2020a. Enhanced H-abstraction contribution for oxidation of xylenes via mineral particles: implications for particulate matter formation and human health. Environ. Res. 186, 109568.

Chen, J.Y., Zhang, Z.L., Zhu, W.K., Zhang, L.Y., Zhao, B.C., Ji, Y.M., Li, G.Y., An, T.C., 2021. Superoxide radical enhanced photocatalytic performance of styrene alters its degradation mechanism and intermediate health risk on TiO_2/graphene surface. Environ. Res. 195, 110747.

Chen, L.C., Cui, W., Li, J.Y., Wang, H., Dong, X.A., Chen, P., Zhou, Y., Dong, F., 2020b. The high selectivity for benzoic acid formation on $Ca_2Sb_2O_7$ enables efficient and stable toluene mineralization. Appl. Catal. B: Environ. Times 271, 118948.

Chen, X.Y., Yao, J.J., Xia, B., Gan, J.Y., Gao, N.Y., Zhang, Z., 2020c. Influence of pH and DO on the ofloxacin degradation in water by UVA-LED/TiO_2 nanotube arrays photocatalytic fuel cell: mechanism, ROSs contribution and power generation. J. Hazard Mater. 383, 121220.

Chen, Y.H., Zhang, J., Tang, Z.Y., Sun, Y.H., 2020d. Visible light catalyzed anti-markovnikov hydration of styrene to 2-phenylethanol: from batch to continuous. J. Photochem. Photobiol. Chem. 392, 112340.
Chen, Z., Peng, Y., Chen, J.J., Wang, C.Z., Yin, H.B., Wang, H.M., You, C.F., Li, J.H., 2020e. Performance and mechanism of photocatalytic toluene degradation and catalyst regeneration by thermal/UV treatment. Environ. Sci. Technol. 54 (22), 14465–14473.
Cheng, Z.W., Feng, L., Chen, J.M., Yu, J.M., Jiang, Y.F., 2013a. Photocatalytic conversion of gaseous ethylbenzene on lanthanum-doped titanium dioxide nanotubes. J. Hazard Mater. 254–255, 354–363.
Cheng, Z.W., Feng, L., Chen, J.M., Yu, J.M., Jiang, Y.F., 2013b. Photocatalytic conversion of gaseous ethylbenzene on lanthanum-doped titanium dioxide nanotubes. J. Hazard Mater. 254, 354–363.
Cheng, Z.W., Sun, P.F., Lu, L.C., Chen, J.M., Jiang, L.Y., Yu, J.M., 2014. The interaction mechanism and characteristic evaluation of ethylbenzene/chlorobenzene binary mixtures treated by ozone-assisted UV_{254nm} photodegradation. Sep. Purif. Technol. 132, 62–69.
d' Hennezel, O., Pichat, P., F Ollis, D., 1998. Benzene and toluene gas-phase photocatalytic degradation over H_2O and HCL pretreated TiO_2: by-products and mechanisms. J. Photochem. Photobiol. Chem. 118, 197–204.
Doucet, N., Zahraa, O., Bouchy, M., 2007. Kinetics of the photocatalytic degradation of benzene. Catal. Today 122 (1–2), 168–177.
Einaga, H., Mochiduki, K., Teraoka, Y., 2013. Photocatalytic oxidation processes for toluene oxidation over TiO_2 catalysts. Catalysts 3 (1), 219–231.
Fotiou, T., Triantis, T.M., Kaloudis, T., O'Shea, K.E., Dionysiou, D.D., Hiskia, A., 2016. Assessment of the roles of reactive oxygen species in the UV and visible light photocatalytic degradation of cyanotoxins and water taste and odor compounds using C-TiO_2. Water Res. 90, 52–61.
Fu, S.F., Zheng, Y., Zhou, X.B., Ni, Z.M., Xia, S.J., 2019. Visible light promoted degradation of gaseous volatile organic compounds catalyzed by Au supported layered double hydroxides: influencing factors, kinetics and mechanism. J. Hazard Mater. 363, 41–54.
Gonzalez-Martin, J., Kraakman, N.J.R., Perez, C., Lebrero, R., Munoz, R., 2021. A state-of-the-art review on indoor air pollution and strategies for indoor air pollution control. Chemosphere 262, 128376.
Guo, H., Lee, S.C., Chan, L.Y., Li, W.M., 2004. Risk assessment of exposure to volatile organic compounds in different indoor environments. Environ. Res. 94 (1), 57–66.
Guo, T., Bai, Z.P., Wu, C., Zhu, T., 2008. Influence of relative humidity on the photocatalytic oxidation (PCO) of toluene by TiO_2 loaded on activated carbon fibers: PCO rate and intermediates accumulation. Appl. Catal. B: Environ 79 (2), 171–178.
Guo, X.Y., Li, Q.L., Zhang, M., Long, M.C., Kong, L.L., Zhou, Q.X., Shao, H.Q., Hu, W.L., Wei, T.T., 2015. Enhanced photocatalytic performance of N-nitrosodimethylamine on TiO_2 nanotube based on the role of singlet oxygen. Chemosphere 120, 521–526.
Jafari, A.J., Kalantari, R.R., Kermani, M., Firooz, M.H., 2020. ZnO nanoparticles photocatalytic activity toward atmospheric toluene under simulated sunlight. Res. Chem. Intermed. 46 (1), 119–131.
Kim, M.S., Liu, G., Cho, H.K., Kim, B.W., 2011. Application of a hybrid system comprising carbon-doped TiO_2 film and a ceramic media-packed biofilter for enhanced removal of gaseous styrene. J. Hazard Mater. 190 (1–3), 537–543.
Kim, S.B., Hwang, H.T., Hong, S.C., 2002. Photocatalytic degradation of volatile organic compounds at the gas–solid interface of a TiO_2 photocatalyst. Chemosphere 48, 437–444.
Kunene, A., Heerden, T., Gambu, T.G., Steen, E., 2020. Liquid phase, aerobic oxidation of benzyl alcohol over the catalyst system (Pt/TiO_2+H_2O). ChemCatChem 12 (19), 4760–4764.
Li, K.Q., Jing, Y.Q., Yang, C.H., Liu, S.S., Zhao, Y.X., He, X.B., Li, F., Han, J.Y., Li, G., 2014. Increased leukemia-associated gene expression in benzene-exposed workers. Sci. Rep. 4, 5369.
Li, X.J., S Jenks, W., 2000. Isotope studies of photocatalysis: dual mechanisms in the conversion of anisole to phenol. J. Am. Chem. Soc. 122 (48), 11864–11870.
Li, Y., Wen, B., Ma, W.H., Chen, C.C., Zhao, J.C., 2012a. Photocatalytic degradation of aromatic pollutants: a pivotal role of conduction band electron in distribution of hydroxylated intermediates. Environ. Sci. Technol. 46 (9), 5093–5099.
Li, Y., Wen, B., Yu, C.L., Chen, C.C., Ji, H.W., Ma, W.H., Zhao, J.C., 2012b. Pathway of oxygen incorporation from O_2 in TiO_2 photocatalytic hydroxylation of aromatics: oxygen isotope labeling studies. Chem.-A Eur. J 18 (7), 2030–2039.
Liang, C., Feng, H.P., Niu, H.Y., Niu, C.G., Li, J.S., Huang, D.W., Zhang, L., Guo, H., Tang, N., Liu, H.Y., 2020. A dual transfer strategy for boosting reactive oxygen species generation in ultrathin Z-scheme heterojunction driven by electronic field. Chem. Eng. J. 384, 123236.
Long, J.L., Xie, X.Q., Xu, J., Gu, Q., Chen, L.M., Wang, X.X., 2012. Nitrogen-Doped graphene nanosheets as metal-free catalysts for aerobic selective oxidation of benzylic alcohols. ACS Catal. 2 (4), 622–631.
Lyu, J., Zhou, L.L., Shao, J.W., Zhou, Z., Gao, J.X., Li, J., Dong, Y.M., Wang, Z.Y., 2020. Synthesis of $TiO_2/H_2Ti_3O_7$ composite with nanoscale spiny hollow hierarchical structure for photocatalytic mineralization of VOCs. Chem. Eng. J. 400, 125927.
Mamaghani, A.H., Haghighat, F., Lee, C., 2018. Photocatalytic degradation of VOCs on various commercial titanium dioxides: impact of operating parameters on removal efficiency and by-products generation. Build. Environ. 138, 275–282.
McKenzie, L.M., Witter, R.Z., Newman, L.S., Adgate, J.L., 2012. Human health risk assessment of air emissions from development of unconventional natural gas resources. Sci. Total Environ. 424, 79–87.
Mendez-Roman, R., Cardona-Martınez, N., 1998. Relationship between the formation of surface species and catalyst deactivation during the gas-phase photocatalytic oxidation of toluene. Catal. Today 40, 353–365.
Michail, K., Siraki, A.G., 2012. Post-trapping derivatization of radical-derived EPR-silent adducts: application to free radical detection by HPLC/UV in chemical, biochemical, and biological systems and comparison with EPR spectroscopy. Anal. Chem. 84 (15), 6739–6746.
Minella, M., Minero, C., 2021. Evaluation of gas/solid photocatalytic performance for the removal of VOCs at ppb and sub-ppb levels. Chemosphere 272, 129636.
Mo, J.H., Zhang, Y.P., Xu, Q.J., Zhu, Y.F., Lamson, J.J., Zhao, R.Y., 2009. Determination and risk assessment of by-products resulting from photocatalytic oxidation of toluene. Appl. Catal. B: Environ. Times 89 (3–4), 570–576.
Mohanta, D., Ahmaruzzaman, M., 2020. A novel Au-SnO_2-rGO ternary nanoheterojunction catalyst for UV-LED induced photocatalytic degradation of clothianidin: identification of reactive intermediates, degradation pathway and in-depth mechanistic insight. J. Hazard Mater. 397, 122685.
Oh, Y., Bao, Y., Jenks, W.S., 2003. Isotope studies of photocatalysis. J. Photochem. Photobiol. Chem. 161 (1), 69–77.
Oturan, M.A., Aaron, J., 2014. Advanced oxidation processes in water/wastewater treatment: principles and applications. a review. Crit. Rev. Environ. Scie. Technol. 44 (23), 2577–2641.
Pang, X.B., Chang, W., Chen, C.C., Ji, H.W., Ma, W.H., Zhao, J.C., 2014. Determining the TiO_2-photocatalytic aryl-ring-opening mechanism in aqueous solution using oxygen-18 labeled O_2 and H_2O. J. Am. Chem. Soc. 136 (24), 8714–8721.
Pelaez, M., Nolan, N.T., Pillai, S.C., Seery, M.K., Falaras, P., Kontos, A.G., Dunlop, P.S.M., Hamilton, J.W.J., Byrne, J.A., O'Shea, K., Entezari, M.H., Dionysiou, D.D., 2012. A review on the visible light active titanium dioxide photocatalysts for environmental applications. Appl. Catal. B: Environ. Times 125, 331–349.
Qiu, L., Wang, Y.N., Li, H., Cao, G., Ouyang, F., Zhu, R.S., 2018. Photocatalytic oxidation of toluene on fluorine doped TiO_2/SiO_2 catalyst under simulant sunlight in a flat reactor. Catalysts 8 (12), 596.
Quici, N., Vera, M.L., Choi, H., Puma, G.L., Dionysiou, D.D., Litter, M.I., Destaillats, H., 2010. Effect of key parameters on the photocatalytic oxidation of toluene at low concentrations in air under 254+185 nm UV irradiation. Appl. Catal. B: Environ. Times 95 (3–4), 312–319.
Rao, Z.P., Shi, G.S., Wang, Z., Mahmood, A., Xie, X.F., Sun, J., 2020. Photocatalytic degradation of gaseous VOCs over Tm^{3+}-TiO_2: revealing the activity enhancement mechanism and different reaction paths. Chem. Eng. J. 395, 125078.
Shah, A.P., Sharma, A.S., Sharma, V.S., Shimpi, N.G., 2020. Polyacrylonitrile nanofibers incorporating silver-decorated graphitic carbon nitride for the visible-light-activated selective oxidation of styrene, benzylic methylene groups, and benzene. ACS Appl. Nano Mater 3 (2), 1922–1933.
Shayegan, Z., Haghighat, F., Lee, C., 2020. Surface fluorinated Ce-doped TiO_2 nanostructure photocatalyst: a trap and remove strategy to enhance the VOC removal from indoor air environment. Chem. Eng. J. 401, 125932.
Shayegan, Z., Lee, C., Haghighat, F., 2018. TiO_2 photocatalyst for removal of volatile organic compounds in gas phase – a review. Chem. Eng. J. 334, 2408–2439.
Shayegan, Z., Lee, C., Haghighat, F., 2019. Effect of surface fluorination of P25-TiO_2 coated on nickel substrate for photocatalytic oxidation of methyl ethyl ketone in indoor environments. J. Environ. Chem. Eng 7 (5), 103390.
Sheng, Z.Y., Ma, D.R., He, Q., Wu, K., Yang, L., 2019. Mechanism of photocatalytic toluene oxidation with $ZnWO_4$: a combined experimental and theoretical investigation. Catal. Sci. Technol 9 (20), 5692–5697.
Shi, T., Chang, W., Zhang, H.N., Ji, H.W., Ma, W.H., Chen, C.C., Zhao, J.C., 2015. H_2O-involved two-electron pathway for photooxidation of aldehydes on TiO_2: an isotope labeling study. Environ. Sci. Technol. 49 (5), 3024–3031.
Sleiman, M., Conchon, P., Ferronato, C., Chovelon, J., 2009. Photocatalytic oxidation of toluene at indoor air levels (ppbv): Towards a better assessment of conversion, reaction intermediates and mineralization. Appl. Catal. B: Environ 86 (3–4), 159–165.
Sun, L., Li, G.Y., Wan, S.G., An, T.C., 2010. Mechanistic study and mutagenicity assessment of intermediates in photocatalytic degradation of gaseous toluene. Chemosphere 78 (3), 313–318.
Vali, A., Malayeri, H.Z., Azizi, M., Choi, H., 2020. DPV-assisted understanding of TiO_2 photocatalytic decomposition of aspirin by identifying the role of produced reactive species. Appl. Catal. B: Environ. Times 266, 118646.
Wei, P., Qin, D.D., Chen, J.Y., Li, Y.X., Wen, M.C., Ji, Y.M., Li, G.Y., An, T.C., 2019. Photocatalytic ozonation mechanism of gaseous n-hexane on MO_x–TiO_2–foam nickel composite (M = Cu, Mn, Ag): unveiling the role of ·OH and $·O_2^-$. Environ. Sci.: Nano 6 (3), 959–969.
Xin, X.D., Sun, S.H., Zhou, A.R., Wang, M.Q., Song, Y., Zhao, Q.H., Jia, R.B., 2020. Sulfadimethoxine photodegradation in UV-C/H_2O_2 system: reaction kinetics, degradation pathways, and toxicity. J. Water Process Eng 36, 101293.
Zhang, M., Wang, Q., Chen, C.C., Zang, L., Ma, W.H., Zhao, J.C., 2009. Oxygen atom transfer in the photocatalytic oxidation of alcohols by TiO_2: oxygen isotope studies. Angew Chem. Int. Ed. Engl. 48 (33), 6081–6084.
Zhou, W., Guan, Z., Zhao, M., Li, J.W., 2019. Characteristics and mechanism of toluene removal from gas by novelty array double dielectric barrier discharge combined with TiO_2/Al_2O_3 catalyst. Chemosphere 226, 766–773.